

Oceanographic Constraints on Exoplanet Life

STEPHANIE L. OLSON,^{1,2} MALTE JANSEN,¹ AND DORIAN S. ABBOT¹

¹*Department of the Geophysical Sciences, University of Chicago*

²*NASA Astrobiology Institute Alternative Earths Team*

(Received; Revised; Accepted)

Submitted to ApJ

ABSTRACT

Liquid water oceans are at the center of our search for life on exoplanets because water is a strict requirement for life as we know it. However, oceans are dynamic habitats—and some oceans may be better hosts for life than others. In Earth’s ocean, circulation transports essential nutrients such as phosphate and is thus a first-order control on the distribution and productivity of life. Of particular importance is upwelling in response to wind-driven divergence in surface layers, which returns essential nutrients that tend to gravitationally accumulate at depth via the biological pump back to the sunlit regions where life is concentrated. The atmospheric accumulation of biogenic gases like methane that are produced in the subsurface marine environment also depends on ocean upwelling, and sea-air transfer of biogenic gases is further modulated by the areal extent of sea ice. Ocean circulation patterns and other oceanographic properties are likely to impose constraints on the activity and atmospheric expression of photosynthetic life in exo-oceans as well, but we lack an understanding of how ocean dynamics may differ on other planets. We address this issue here by exploring the sensitivity of ocean dynamics. We use ROCKE-3D, a fully coupled ocean-atmosphere GCM, to quantify ocean upwelling, surface mixed layer depth, and sea ice coverage over a broad range of planetary conditions. We determine how each of these biogeochemically important oceanographic properties varies with a planet’s surface pressure, rotation rate, radius, orbital obliquity, stellar irradiation, and ocean salinity. Our results suggest that planets that rotate slower and have higher surface pressure than Earth may be the most attractive targets for remote life detection because upwelling is enhanced under these conditions, resulting in greater nutrient supply to the surface biosphere. Seasonal deepening of the mixed layer on high obliquity planets may also enhance nutrient replenishment from depth into the surface mixed layer. Efficient nutrient recycling favors greater biological activity, more biosignature production, and thus more detectable life. We also argue that an absence of continents is likely to be particularly problematic for sustaining a globally active, remotely detectable marine biosphere due to limited nutrient fluxes from coastal upwelling and continental weathering. More generally, our results demonstrate the importance of considering oceanographic phenomena for exoplanet life detection and motivate future interdisciplinary contributions to the emerging field of exo-oceanography.

Keywords: Astrobiology, Exoplanets, Ocean-atmosphere interactions

1. INTRODUCTION

Water is an essential ingredient for life as we know it. For this reason, the potential existence of a liquid water ocean defines the Habitable Zone concept that guides

our search for life in the Universe (Kasting et al. 1993). However, oceans are dynamic habitats—and oceanographic processes have additional and far-reaching implications for habitability that remain largely unexplored. Recent studies have investigated the importance of considering ocean heat transport for regulating climate and elucidating the boundaries of the Habitable Zone (Hu & Yang 2014; Cullum et al. 2014, 2016; Yang

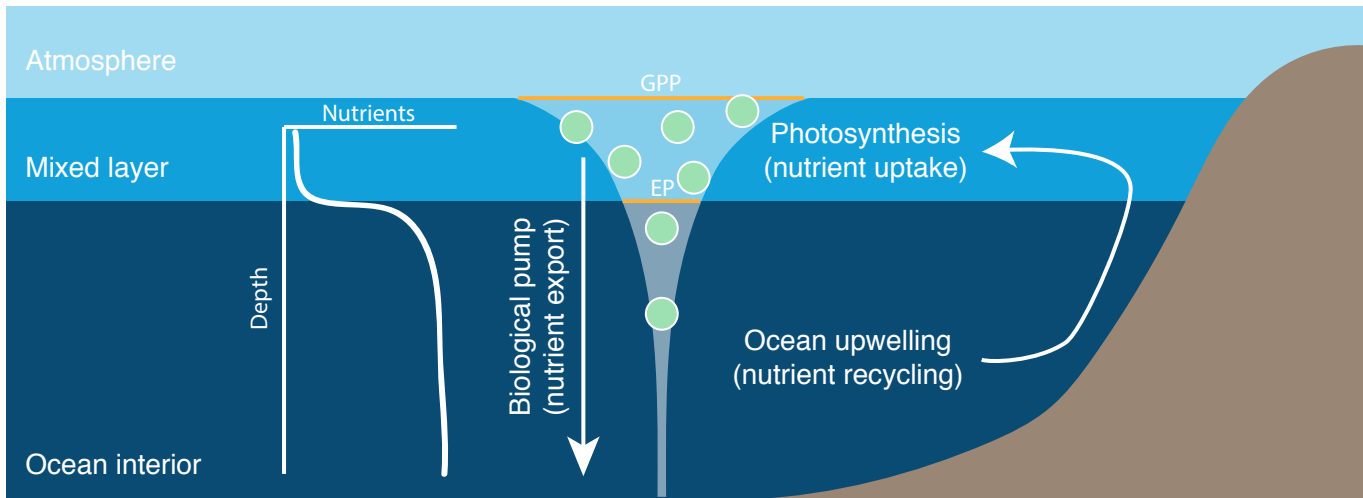
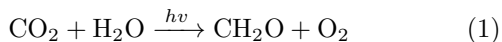


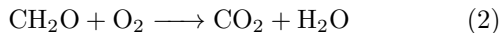
Figure 1. Schematic of ocean nutrient cycling. Nutrients such as phosphate are consumed by photosynthetic life in the sunlit portion of the ocean and are gravitationally exported to depth through the settling of particulate organics, resulting in surface waters that are nutrient-depleted and deep waters that are nutrient-rich. The fraction of total biomass production (Gross Primary Productivity; GPP) that settles out of the mixed layer is referred to as export production (EP). EP allows the isolation of photosynthetic O_2 and reduced organic carbon, which is essential for both the surface accumulation of O_2 and the production of reduced biogenic gases like CH_4 at depth in Earth’s ocean—but EP also removes nutrients from the surface environment and necessitates that nutrients are recycled via ocean upwelling to sustain the biosphere.

et al. 2019), but the significance of ocean circulation is not limited to climate influences.

Ocean circulation is also a primary control on the distribution of biological activity at Earth’s surface as a consequence of the biological pump. Briefly, life in Earth’s ocean is concentrated in the shallow sunlit portion of the water column where photosynthesis is viable. The chemical reaction corresponding to photosynthesis can be represented as:



where CH_2O is a simple representation of biomass. In reality, biomass is chemically complex and includes a number of additional bioessential elements (nutrients), including N and P, and it has a C:N:P ratio of 106:16:1 on average today. The availability of essential nutrients thus limits the amount of photosynthesis that can occur. The majority of photosynthetic biomass is degraded by respiration



in the shallow ocean but a small fraction escapes degradation by settling through the water column, bringing the nutrients consumed during photosynthesis with it. This export of organic particulates from the shallow ocean, referred to as the ‘biological pump,’ preserves the chemical disequilibrium produced from stellar energy during photosynthesis by physically separating reduced organic carbon from photosynthetic O_2 . Separation of reduced C and photosynthetic O_2 stimulates

a diversity of microbial metabolisms within the ocean interior and marine sediments, including methanogenesis. Export production is thus essential for the oxygenation of our atmosphere and the net production of other putative biosignature gases such as CH_4 on Earth, but efficient removal of biomass from the sunlit portion of the ocean requires a mechanism for replenishing nutrients lost to depth. The primary mechanism for nutrient replenishment to the mixed layer of Earth’s ocean is upwelling, or upward flow of deep water to the surface ocean.

Upwelling is a wind-driven phenomenon that occurs in regions where the horizontal ocean current diverges. Conservation of mass requires upwelling of water from below in response to this divergence. For example, upwelling occurs where winds drive ocean currents off the coast of a continent that obstructs lateral flow. Upwelling also occurs at low latitudes as the consequence of opposing directions of Coriolis deflection on either side of the equator. Vertical mixing of the ocean is otherwise disfavored because the ocean is stably stratified with respect to density, with warm, less dense water on top of cold, denser water. A critical impact of upwelling is that it brings nutrient-rich water up to the surface from the deep ocean. As a result, photosynthetic life is overwhelmingly concentrated in upwelling regions of Earth’s ocean today. This cycle of nutrient uptake in the shallow ocean, export to depth, and recycling via upwelling is summarized in Figure 1.

The importance of surface winds is not limited to their role in large-scale ocean circulation patterns. The winds also influence global biogeochemical cycles through their impact on the mixed layer depth. The mixed layer is the portion of the water column that is homogenized by turbulence and is in contact with the overlying atmosphere. It represents less than 10% of the global ocean volume. Deepening of the mixed layer reduces the average light levels a photosynthetic cell experiences in its lifetime and upon death may increase its exposure time to photosynthetic or photochemically derived oxidants that favor its decomposition. In sum, very deep mixed layers may reduce gross primary productivity (GPP) via light inhibition as well as export production (EP) via enhanced recycling internal to the mixed layer (Sverdrup 1953; Li & Cassar 2017), ultimately limiting net production of biosignature gases like O_2 and CH_4 that depend on the physical separation of photosynthetic oxidants and reduced organic matter. A mixed layer that is shallow compared to light penetration depths may thus favor remotely detectable biospheres by enhancing productivity and export—but, ironically, efficient export reinforces the critical importance of ocean upwelling for sustaining biospheric productivity by returning nutrients to the surface.

Although life on other planets is likely to differ from life on Earth, photosynthetic life will require nutrients for the construction of its biomolecules regardless of the details of its biochemistry. Moreover, it is likely that these nutrients would tend to gravitationally accumulate at depth in exo-oceans. It is thus reasonable to expect that ocean circulation patterns may be a first-order control on the activity of photosynthetic life on inhabited exoplanets as well. These relationships have practical implications for the detectability of life elsewhere because the most active surface biospheres with the greatest export fractions will have the greatest potential to influence the spectral appearance of their host planets and will thus be the most detectable biospheres (Schwieterman et al. 2018; Krissansen-Totton et al. 2018). Conversely, subsurface life, low productivity biospheres, biospheres in which biosignatures are either accumulated at depth or efficiently recycled within the ocean will be very challenging to detect because biosignature production and communication to the atmosphere will be limited under these circumstances.

Productive biospheres are an insufficient prerequisite for detectability because biogenic gases within the ocean will not be recognizable with telescopes. Remotely detectable marine biospheres also require the transport of biogenic gases from the ocean environment to the atmosphere via sea-air gas exchange. For example, the global

sea-to-air flux of O_2 is described by:

$$F_{O_2} = k_{O_2} A (1 - f_{ice}) ([O_2] - [O_2]_{sat}), \quad (3)$$

where A is the surface area of the ocean, f_{ice} is the fractional ice cover, $[O_2] - [O_2]_{sat}$ reflects oceanic O_2 super- or under-saturation with respect to the overlying atmosphere, and k_{O_2} is the O_2 gas exchange constant. k_{O_2} is sensitive to wind stress and sea surface temperature. If the exchange flux of O_2 is small compared to biological fluxes within the ocean and/or its destruction within the atmosphere, disequilibrium between the ocean and the atmosphere can be maintained (Olson et al. 2013) with potentially important ramifications for remote life detection, including the possibility of ‘false negatives’ for life despite large-scale biological O_2 production (Reinhard et al. 2017a). Similarly, extensive biological production of CH_4 in the ocean does not necessarily manifest as high levels of atmospheric CH_4 because biological CH_4 oxidation internal to the ocean may severely limit its flux to the atmosphere (Olson et al. 2016), depending on oxidant availability, ocean upwelling rates, and the areal extent of sea ice.

Despite their importance, we lack a rigorous understanding of how ocean upwelling, the mixed layer depth, and the transfer of marine biosignatures to the atmosphere may differ among the diversity of habitable exoplanets. In other words, we do not know which planetary scenarios are most conducive to the development of remotely detectable oceanic biospheres—or whether these scenarios are observationally distinguishable. Placing constraints on exo-ocean circulation patterns would aid in identifying the most favorable targets for detailed characterization. This knowledge would also provide useful context for evaluating the vulnerability of a particular planet to a biosignature false negative and assist in assigning significance to inherently ambiguous non-detections (Reinhard et al. 2017a).

Whereas detecting exo-oceans will be feasible with future instruments (Robinson et al. 2010; Lustig-Yaeger et al. 2018), directly characterizing ocean dynamics and marine habitats will not be possible. It is thus necessary to understand the sensitivity of ocean circulation patterns to observable planetary parameters—and to understand the uncertainty introduced by other factors that may be difficult to constrain remotely. As a first step, we use a general circulation model (GCM) to quantify the sensitivity of global upwelling and other biogeochemically significant oceanographic quantities to a broad range of planetary parameters (Sections 3.1–3.6). We then discuss how these oceanographic constraints may affect biospheric productivity and the detectability of life on inhabited planets differing from our own

(Section 4.1). We conclude by offering recommendations regarding the most favorable targets for exoplanet life detection and observational prospects for assessing the likelihood of a false vs. true negative in the face of an ambiguous non-detection (Section 4.2).

2. MODEL DESCRIPTION

We perform our calculations using ROCKE-3D (Way et al. 2017), a fully coupled ocean-atmosphere GCM that is modified from the NASA Goddard Institute for Space Studies (GISS) ModelE2 (Schmidt et al. 2014). See Way et al. (2017) for a detailed description of ROCKE-3D and its parent model. The model is publicly available from the NASA GISS ModelE repository.

Our ROCKE-3D simulations use $4^\circ \times 5^\circ$ latitude-longitude resolution with 40 vertical layers in the atmosphere (up to 0.1 mbar) and 10 depth layers in the ocean (down to 1360 m). We spun up each model scenario to a steady-state, which we diagnosed by the achievement of a global radiative balance of $0 \pm 0.2 \text{ W m}^{-2}$ averaged over the last 10 years of the run. We further confirmed steady-state by checking for stable temperature and salinity in the abyssal ocean. Radiative balance was typically achievable in 500 model years, but reaching steady-state required modestly longer run times for some model scenarios. All of the data we show are averaged over the last 10 years of each simulation independent of the total run time.

2.1. Baseline planet

Our ‘baseline planet’ configuration resembles present-day Earth in many ways (see Table 1). We adopt Earth values for the mass, radius, and surface gravity of our baseline planet. Additionally, our baseline planet has a 24-hour rotation period and orbits a sun-like star with a 365-day period. Our baseline planet receives an Earth-like stellar irradiation of 1360 W m^{-2} , but we assume that the planet’s obliquity and eccentricity are both zero to eliminate complications arising from seasonally variable irradiation. This choice ultimately reduces run times and allows a greater exploration of parameter space.

Like Earth, our baseline planet has a surface pressure of 1 atm at sea level. Unlike Earth, however, our baseline planet lacks O_2 (and O_3) and instead has an N_2 atmosphere (>99%) with trace (pre-industrial) levels of CO_2 and CH_4 . The combination of zero obliquity and modest CO_2 yields a climate that is somewhat cooler than that of present-day Earth, particularly at high latitudes, but is nonetheless Earth-like and habitable (Figure 2).

The distribution of land masses and ocean bathymetry on our baseline planet is based on present-day Earth

Table 1. Baseline planet parameters

Parameter	Baseline
Rotation period	24 hours
Orbital period	365 days
Mass	M_\oplus
Radius	r_\oplus
Surface gravity	9.8 m/s^2
Surface pressure	1 atm
Obliquity	0°
Eccentricity	0°
Stellar spectrum	Sun
Stellar irradiation	1360 W m^{-2}
Map	Modified Earth
Ocean depth	1360 m
Salinity	35 PSU

with a few exceptions (Figure 2). Most notably, we have implemented a ‘bathtub’ ocean bathymetry (Way et al. 2018). This ocean has deepened shelves (591 m) compared to our ocean and it has a flat bottom that is shallower than Earth’s ocean (1360 m). Moreover, this ocean bathymetry eliminates several small and/or shallow seas such as the Mediterranean, Baltic, Black Sea, Red Sea, and Hudson Bay by designating these areas as landmass. Unlike Way et al. (2018), we have also eliminated Baffin Bay by removing the island of Greenland. In combination, these changes to the continental configuration and ocean bathymetry allow examination of a greater diversity of habitable climates by avoiding stability issues that arise on icy planets (Way et al. 2018). An aquaplanet would impart similar benefits, but our approach is preferable to using an aquaplanet configuration because it allows us to examine the biogeochemically significant phenomenon of coastal upwelling.

2.2. Sensitivity experiments

We examine model sensitivity to: radius, surface pressure, rotation rate, obliquity, stellar irradiation, and ocean salinity. We change each parameter from our baseline experiment in isolation, with the exception of a few parameters that we co-vary for self-consistency. We outline our procedures and underlying assumptions for these experiments below, and Table 2 summarizes the ranges for each parameter.

We vary planet radius up to 2x Earth’s radius (r_\oplus). This is a narrow range compared to the radii of known exoplanets, but it is generously inclusive of the radii of planets that are potentially rocky and Earth-like (Rogers 2015). Upon changing radius, we

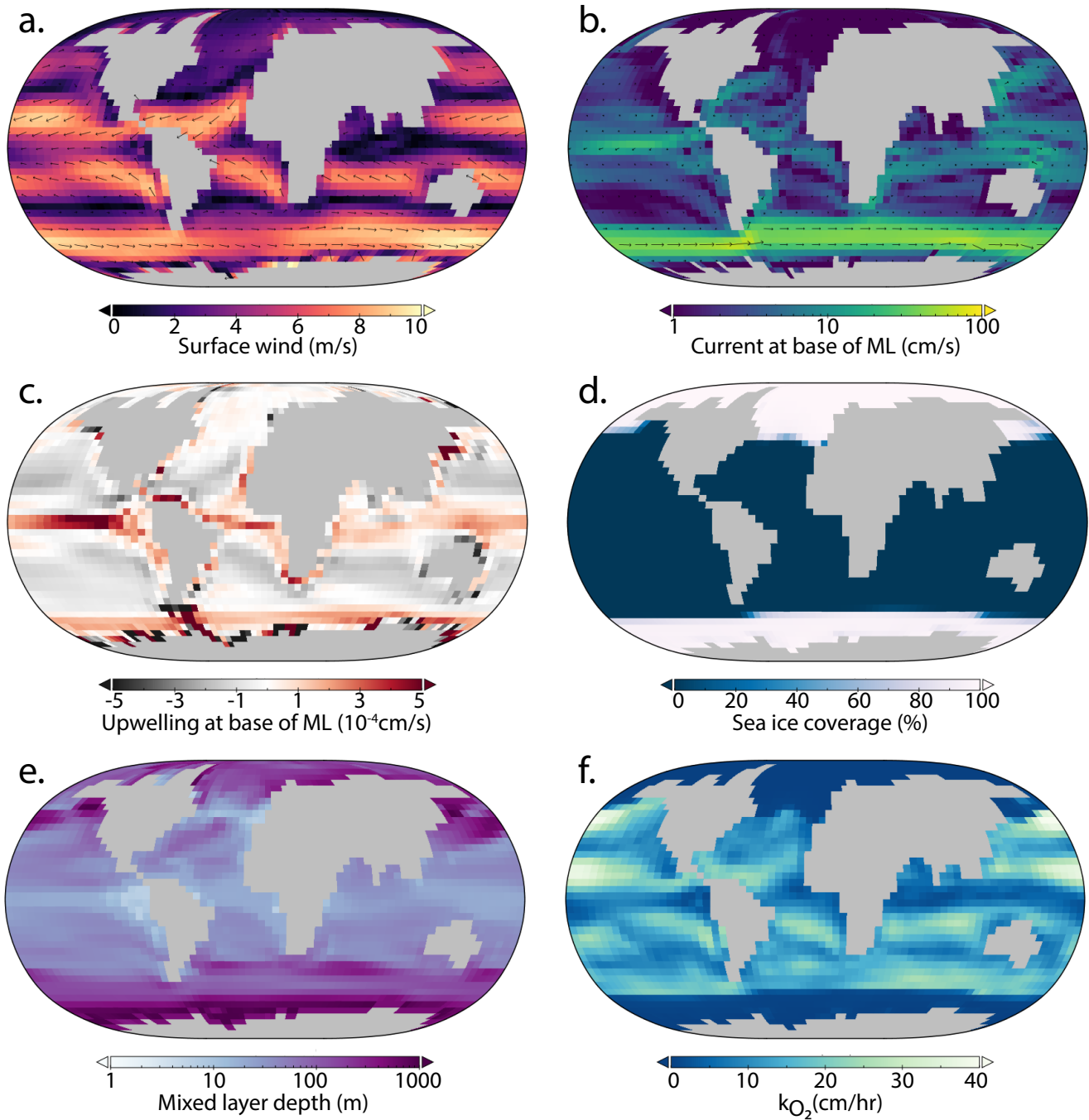


Figure 2. Key oceanographic parameters for the Earth-like baseline planet. Shown are: surface winds (a), ocean currents at the base of the mixed layer (b), vertical velocities (upwelling) at the base of the mixed layer (c), sea ice coverage (d), mixed layer depth (e), and the oxygen exchange coefficient (f).

Table 2. Sensitivity Experiments

Parameter	Minimum	Maximum
Rotation period	12 hours	10 days
Radius	r_{\oplus}	$2r_{\oplus}$
Surface pressure	0.5 atm	10 atm
Stellar irradiation	1000 w/m ²	1500 w/m ²
Obliquity	0°	45°
Salinity	3.5 PSU	70 PSU

self-consistently update planet mass, surface gravity, and surface pressure. Following the empirical relationship derived by [Kopparapu et al. \(2014\)](#), we assume that planetary mass is related to its radius by:

$$\left(\frac{M_p}{M_b}\right) = 0.968 \left(\frac{r_p}{r_b}\right)^{3.2} \quad (4)$$

where M_b and r_b are the mass and radius of our baseline planet (M_b and r_b are equal to M_{\oplus} and r_{\oplus} , respectively).

Surface gravity is in turn related to both the planetary mass and radius by:

$$\left(\frac{g_p}{g_b}\right) = \left(\frac{M_p}{M_b}\right) \left(\frac{r_b}{r_p}\right)^2 \quad (5)$$

where g_b refers to the surface gravity on our baseline planet, g_{\oplus} (9.8 m s⁻²).

Surface pressure is proportional to surface gravity, and it is further modulated by the surface area of the planet (A_p) and the mass of the overlying atmosphere (m_p):

$$\left(\frac{P_p}{P_b}\right) = \left(\frac{m_p}{m_b}\right) \left(\frac{g_p}{g_b}\right) \left(\frac{A_b}{A_p}\right) \quad (6)$$

where m_b and A_b represent the surface area and atmospheric mass of our baseline planet. We scale the mass of the atmosphere as the surface area evolves with radius such that $m_p/A_p = m_b/A_b$. Substitution yields:

$$\left(\frac{P_p}{P_b}\right) = 0.968 \left(\frac{r_p}{r_b}\right)^{1.2} \quad (7)$$

We note that this formulation diverges somewhat from that of [Kopparapu et al. \(2014\)](#) because they assumed that m_p is proportional to M_p . This scaling between planetary and atmospheric mass may be a reasonable approximation, but we instead opt to preserve m/A for each of our radius experiments and modify atmospheric mass in isolation in subsequent sensitivity analyses. We did this by changing surface pressure between 0.5 and 10 atm for constant surface gravity, mass, and radius.

2.3. Oceanographic metrics

Our analysis focuses on 10 year global averages of several oceanographic properties of biogeochemical significance:

1. **wind stress.** Wind stress is calculated as

$$\tau = C_D \rho_{atm} U^2, \quad (8)$$

where ρ_{atm} is atmospheric density, which increases proportional to surface pressure for atmospheres of constant composition. U is surface wind speed (m/s). We assume that C_D , the wind drag coefficient, is constant across the planetary parameter space we explore. We exclude land cells from our wind stress calculation but we do not account for sea ice, which modulates the transfer of wind stress to the underlying ocean ([Zhang & Rothrock 2000](#)).

2. **density stratification.** We leverage the surface-to-deep potential density contrast, $\Delta\sigma$, as a proxy for the stability of the density stratification. We simply calculate $\Delta\sigma$ as the average potential density of the surface ocean layer minus the global-average potential density of the bottom ocean layer. Potential density is the density that a parcel of water would have if adiabatically brought to the surface; whereas in situ density varies with depth (pressure) in the ocean, potential density changes does not and instead reflect differences in temperature and salinity. The vertical potential density contrast is a reflection of horizontal equator-to-pole density gradients in the surface ocean because the deep ocean is filled with the densest waters from the surface.
3. **the depth of the mixed layer.** The depth of the mixed layer in ROCKE-3D varies in space and time, and is calculated using the K profile parameterization (KPP) scheme ([Large et al. 1994](#)).
4. **ocean upwelling.** Upwelling is presented as globally summed upwelling at the base of the mixed layer. Although we spatially average the mixed layer depth, our upwelling sum accounts for spatial variability in the depth of the mixed layer and is calculated as the area-weighted sum of upward flow (cm³ s⁻¹) in the depth layers containing the base of the mixed layer for each latitude and longitude position. Summing upwelling at fixed depth yields similar results. Upwelling is classified as equatorial if it occurs in the two latitude bands of grid cells straddling the equator (<4° N/S) and upwelling is classified as coastal if any of the eight

adjacent cells is land. Cells may be counted as both equatorial and coastal, but are only counted once towards the global total.

5. **sea-air gas exchange constant.** We calculate the gas exchange constant for O_2 following Wanninkhof (2014) with minor modifications to account for ice cover and variable surface pressure:

$$k_{O_2} = 0.251(1 - f_{ice})U^2 \left(\frac{P_p}{P_b}\right) \left(\frac{Sc_{O_2}}{660}\right)^{-0.5} \quad (9)$$

where f_{ice} is the fractional ice cover. The Schmidt number, Sc_{O_2} , is equal to 568 at 20 °C and is described by a fourth-order polynomial with respect to sea surface temperature (Wanninkhof 2014).

3. RESULTS

3.1. Rotation rate

Globally integrated upwelling at the base of the mixed layer increases with decreasing rotation rate (equivalently, increasing day length; Figure 3a). For modest changes in rotation rate, changes in upwelling are qualitatively predicted by the expected response of the wind-driven surface ocean ‘Ekman’ transport, which is described by:

$$V = \frac{\tau}{\rho f} \quad (10)$$

where V is the magnitude of the horizontal wind-driven transport integrated over the ocean surface boundary layer and f is the Coriolis parameter. The Coriolis parameter is defined as:

$$f = 2\Omega \sin(\varphi) \quad (11)$$

where Ω represents the planet’s rotation rate and φ is latitude. On global average, f is simply equal to rotation rate. Upwelling is primarily driven by divergence of this wind-driven Ekman transport and should therefore be inversely proportional to rotation rate.

Rotation rate also influences the globally averaged mixed layer depth. The mixed layer depth modestly increases with decreasing rotation rate in our experiments despite slower winds and decreasing wind stress at slow rotation rates (Figure 3b,d). This counter-intuitive result appears to arise because the density stratification of the ocean, which limits the mixed layer depth, is weakened due to enhanced meridional heat transport (Kaspi & Showman 2015; Komacek & Abbot 2019), warmer poles, and smaller equator-to-pole temperature gradients as rotation rate decreases (Figure 3e). Equivalent winds can thus induce deeper mixed layers on more slowly rotating planets.

The global-average coefficient for O_2 exchange with the atmosphere does not respond monotonically to increasing rotation rate. k_{O_2} increases with increasing rotation rate from 0.1–1x Earth’s rotation rate as wind stress increases, but the increase is partially compensated for by cooling and expanding ice. With further increases in rotation rate, the combination of decreasing wind stress and increasing sea ice result in a sharp reduction of sea-air gas exchange.

3.2. Surface pressure

The depth of the mixed layer and global upwelling at the base of the mixed layer increases with increasing surface pressure beyond 1 atm (Figure 4a). This relationship primarily arises from increased wind stress with increasing surface pressure, which allows the winds to exert greater influence on ocean dynamics via Equation 10. Wind stress is also strongly sensitive to surface wind speed (Equation 8). Wind speed decreases with increasing surface pressure, but these changes in wind speed are smaller than the changes in atmospheric density in our experiments. The pressure effect thus dominates the wind stress response (Figure 4d). Greater wind stress contributes to enhanced wind-driven ocean circulation, including surface divergence. The result is more upwelling beneath higher density atmospheres. Deviation from this trend at low surface pressure likely arises due to secondary climatic influences.

Increasing surface pressure initially increases surface temperatures due to pressure broadening, but Rayleigh scattering for surface pressure above 2 atm eventually yields cooling and an expansion of sea ice as surface pressure is increased further (Keles et al. 2018; Komacek & Abbot 2019). Meanwhile, meridional heat transport increases with increasing surface pressure, resulting in a smaller difference between equatorial and polar temperatures (Kaspi & Showman 2015). This reduced latitudinal temperature contrast mutes the vertical density stratification of the ocean on average because the deep ocean is ultimately filled with the densest waters from the surface (Figure 4e).

Sea-air gas exchange is initially favored by increasing surface pressure due to the combined effects of increasing wind stress, warming, and reductions in sea ice cover but at surface pressures much higher than present-day Earth cooling ultimately leads to an expansion of sea ice cover, which limits ocean-atmosphere connectivity.

We note that the surface pressure at which climatic trends reverse will be sensitive to atmospheric composition, and the details of the relationship between surface pressure, climate, and ocean dynamics may differ on planets with differing greenhouse gas abundances.

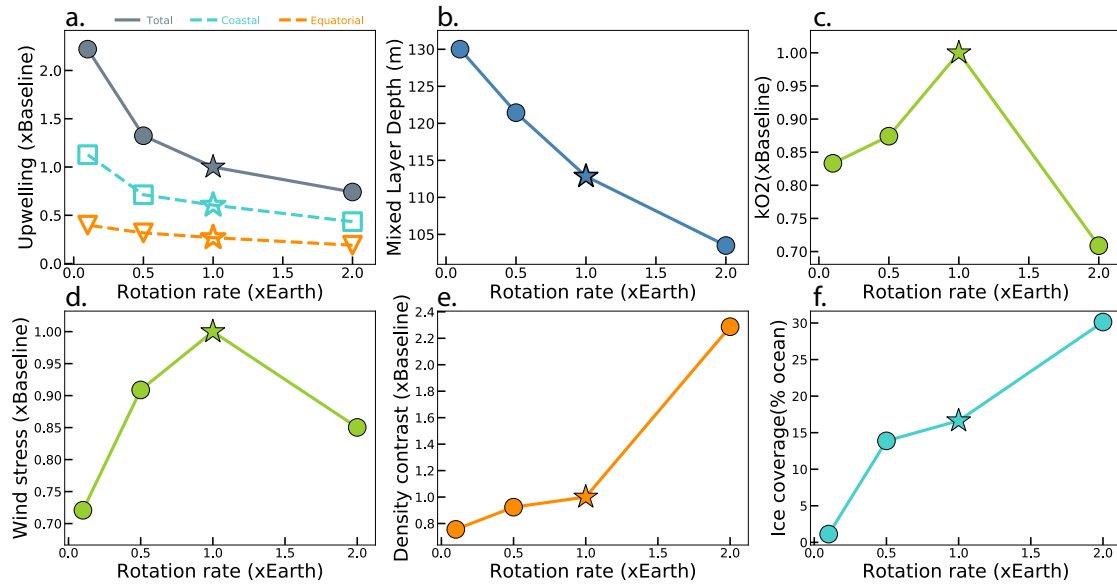


Figure 3. Ocean-atmosphere sensitivity to rotation rate, including: globally summed upwelling at the base of the mixed layer (a), global-average mixed layer depth (b), global-average oxygen gas exchange constant (c), global-average wind stress over ocean cells (d), global-average surface-to-deep density contrast (e), and global sea ice coverage (f). In each panel, the star denotes the Earth-like baseline planet. Upwelling, k_{O_2} , wind stress, and the density contrast are normalized to their baseline values for ease of comparison. In (a), the filled grey circles represent the global total, the open blue squares are the coastal upwelling contribution to that total, and the open orange triangles are the equatorial upwelling component. All data are averaged over the last decade of the simulations.

3.3. Radius

Unlike our other sensitivity analyses, we did not vary planetary mass and radius in isolation; instead, we self-consistently updated mass, gravity, and surface pressure as we changed radius (see discussion in Section 2.2).

We found that global upwelling increases with increasing radius (Figure 5a, filled circles). However, we note that this trend is eliminated when global upwelling is normalized to surface area which increases as r^2 (Figure 5a, open squares). In other words, upwelling per unit area is nearly constant despite an absolute increase in the global sum on larger planets.

The global-average mixed layer depth decreases slightly with increasing radius despite an increase in wind stress (Figure 5b,d). This shallowing of the mixed layer likely arises because ocean stratification is enhanced when surface gravity is increased (Figure 5e). Although we have simplistically adopted $\Delta\sigma$ as a stratification metric for global comparisons between simulations, the dynamically relevant metric is the buoyancy stratification, which is also proportional to g . The open squares in Figure 5e show $g\Delta\sigma$ and reflect the gravitational influence of changing planetary mass and radius on buoyancy stratification. This effect strongly stabi-

lizes stratification in opposition to the effect of increased wind stress on the mixed layer depth.

3.4. Stellar irradiation

Varying stellar irradiation from 1000 to 1500 $W m^{-2}$ assuming constant pCO_2 yields climates that range from snowball states to ice-free states. Global upwelling at the base of the mixed layer does not change monotonically with stellar irradiation across this large range of climate states. Upwelling is optimized at intermediate stellar irradiation: upwelling wanes as the planet enters snowball glaciation and upwelling also decreases in warm climates (Figure 6a). These changes in upwelling generally mirror changes in globally averaged wind stress (Figure 6d), with variable modulation by ice cover that is not accounted for in our wind stress metric (Figure 6f). We note that ROCKE-3D neglects geothermal heat input at the bottom of the ocean, which may be an important influence on ocean dynamics on ice-covered worlds (Ashkenazy et al. 2013; Jansen 2016).

The mixed layer gets shallower with increasing stellar irradiation above the snowball threshold (Figure 6b). This trend is opposite to the relationship between the mixed layer and warming in our other experiments. The reason for this difference is that warming induced by in-

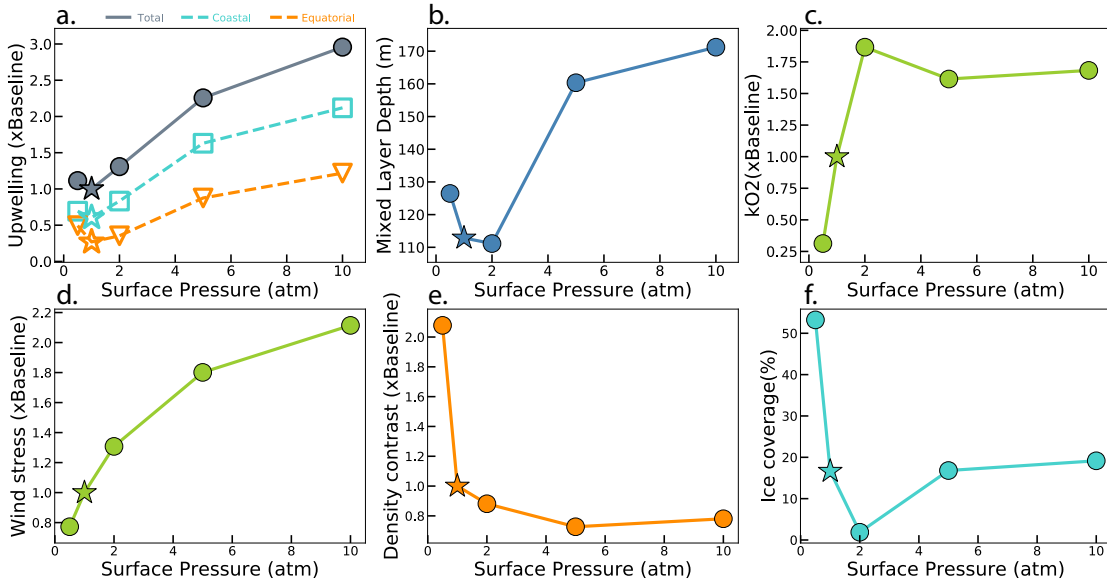


Figure 4. Ocean-atmosphere sensitivity to surface pressure, including: globally summed upwelling at the base of the mixed layer (a), global-average mixed layer depth (b), global-average oxygen gas exchange constant (c), global-average wind stress over ocean cells (d), global-average surface-to-deep density contrast (e), and global sea ice coverage (f). In each panel, the star denotes the Earth-like baseline planet. Upwelling, k_{O_2} , wind stress, and the density contrast are normalized to their baseline values for ease of comparison. In (a), the filled grey circles represent the global total, the open blue squares are the coastal upwelling contribution to that total, and the open orange triangles are the equatorial upwelling component. All data are averaged over the last decade of the simulations.

creasing pressure or reducing rotation rate preferentially warm the poles with respect to the equator by enhancing meridional heat transport and tends to limit the thermal stratification of the ocean. Conversely, warming by increasing stellar irradiation initially warms equatorial waters preferentially compared to polar waters which remain near the freezing point of seawater, exaggerating the equator-to-pole temperature contrast within the ocean. Warming via increased stellar irradiation thus uniquely strengthens thermal stratification in the ocean and results in a shallower mixed layer, even in the face of increasing wind stress (Figure 6d). This relationship breaks down as sea ice retreats and polar waters warm (Figure 6f), but the mixed layer continues shallowing nonetheless because wind stress ultimately decreases in response to weakened temperature gradients.

3.5. Obliquity

Increasing obliquity from 0-45° yields warmer climates and a reduction of sea ice on annual average (Kang 2019; Figure 7f). The equator-to-pole temperature difference is also substantially reduced due to a more equal distribution of stellar irradiation at the planet’s surface, leading to reduced ocean stratification (Figure 7e). Nonethe-

less, the mixed layer depth decreases on annual average with increasing obliquity. This is somewhat unexpected given the dramatic reduction in density stratification (Figure 7e), but may be partially explained by a reduction in wind stress as obliquity increases (Figure 7d). Moreover, the depth of the mixed layer is strongly seasonal, deepening by as much as a factor of 100x in the winter compared to the summer in our 45° obliquity scenario (Figure 8). At high latitudes, the winter mixed layer may extend all the way to the bottom of the ocean introducing the possibility of even deeper mixed layers on planets with deeper oceans.

Globally and annually averaged upwelling increases only slightly with increasing obliquity (Figure 7a). However, extreme seasonal deepening of the mixed layer may allow entrainment of nutrients from depth that is not captured by our upwelling metric. Seasonality in the mixed layer depth is likely to play an important role as a mechanism for nutrient regeneration on high obliquity planets.

3.6. Salinity

Ocean salinity impacts the climate system in several ways. For example, it strongly influences temperature-

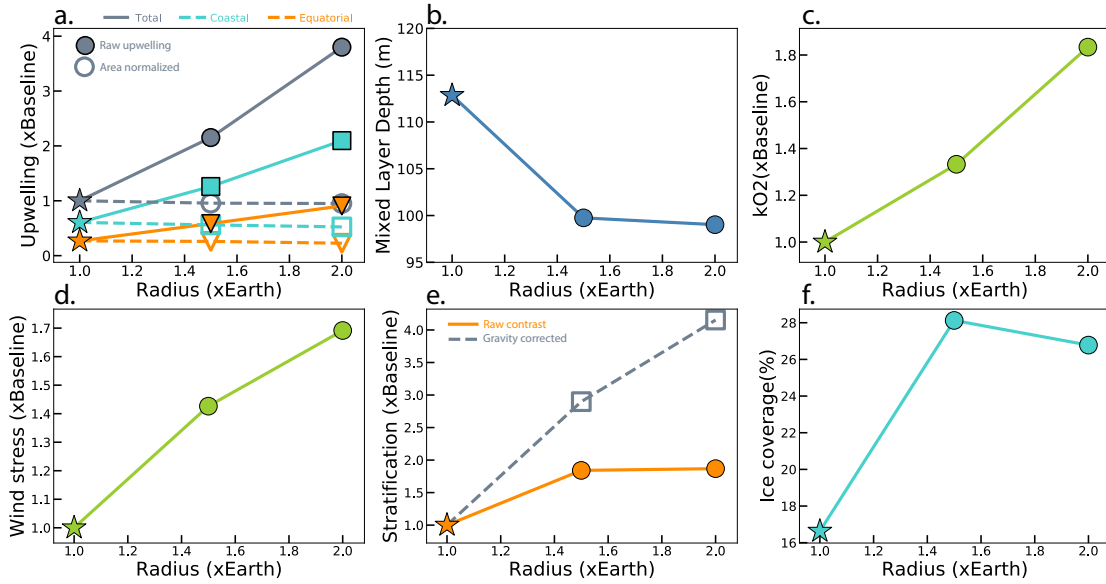


Figure 5. Ocean-atmosphere sensitivity to planet radius, including: globally summed upwelling at the base of the mixed layer (a), global-average mixed layer depth (b), global-average oxygen gas exchange constant (c), global-average wind stress over ocean cells (d), global-average surface-to-deep density contrast (e), and global sea ice coverage (f). In each panel, the star denotes the Earth-like baseline planet. Upwelling, k_{O_2} , wind stress, and the density contrast are normalized to their baseline values for ease of comparison. In (a), the filled grey circles represent the global total, the filled blue squares are the coastal upwelling contribution to that total, and the filled orange triangles are the equatorial upwelling component. The open symbols share the same color and symbol associations with total, coastal, and equatorial upwelling, but these data have been normalized to surface area, which increases as r^2 . In (e), filled circles represent our simple stratification metric, $\Delta\sigma$, as elsewhere in this text, and the open squares have been corrected for gravity influences on buoyancy as planetary radius is increased ($g\Delta\sigma$). All data are averaged over the last decade of the simulations.

density relationships and the density structure of the ocean. However, the most significant impact that varying salinity has on the marine environment in our experiments is its influence on sea ice formation: relatively small increases in salinity result in dramatic reductions in sea ice. There are two reasons. First, salt suppresses the freezing point of seawater and thus directly limits sea ice formation. Moreover, brine rejection during sea ice formation triggers deep convection, which may bring up warmer water from below. Both of these effects interact with the ice-albedo feedback, which tends to amplify changes in ice coverage through associated changes in planetary albedo. Global-average temperature ultimately increases with ocean salinity because the reduction of ice coverage results in a less reflective surface and higher water content of the atmosphere. Doubling ocean salinity compared to present-day Earth precludes sea ice formation and yields 6 K warming on global average (Figure 9f).

The inhibition of freezing and larger thermal expansion coefficient at higher salinities allow for a larger temperature and density contrast, ultimately enhancing

density stratification throughout the ocean (Figure 9e). The result is a shallowing of the mixed layer depth with increasing ocean salinity (Figure 9b). An accompanying reduction of the atmospheric equator-to-pole temperature gradient and wind stress reinforces this effect (Figure 9d).

Upwelling at the base of the mixed layer increases slightly with increasing salinity (Figure 9a). This relationship is surprising given that wind stress decreases as salinity increases as a consequence of reduced temperature gradients. Upwelling might increase as the area of ice-free ocean increases and/or this increase may reflect an increase in brine-driven convection. Indeed, gains in upwelling diminish at high salinity because sea ice is fully eliminated and brine rejection ceases.

Sea-air gas exchange is enhanced with increasing salinity due to warmer temperatures on global average and reduced sea ice cover (Figure 9c,f). Decreasing gas solubility with increasing salinity also favors more efficient transfer of biological gases to the atmosphere from saltier oceans, which would bolster the trend of increasing k_{O_2} with increasing salinity.

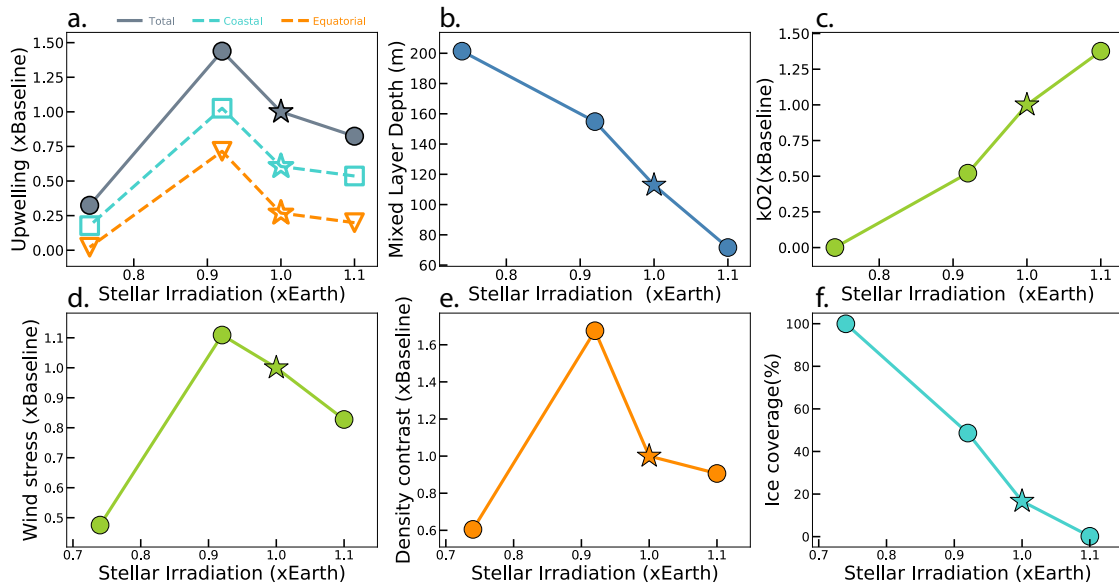


Figure 6. Ocean-atmosphere sensitivity to stellar irradiation, including: globally summed upwelling at the base of the mixed layer (a), global-average mixed layer depth (b), global-average oxygen gas exchange constant (c), global-average wind stress over ocean cells (d), global-average surface-to-deep density contrast (e), and global sea ice coverage (f). In each panel, the star denotes the Earth-like baseline planet. Upwelling, k_{O_2} , wind stress, and the density contrast are normalized to their baseline values for ease of comparison. In (a), the filled grey circles represent the global total, the open blue squares are the coastal upwelling contribution to that total, and the open orange triangles are the equatorial upwelling component. All data are averaged over the last decade of the simulations.

4. DISCUSSION

4.1. Oceanographic constraints on life

We simulated a diversity of habitable ocean environments, some of which may be more hospitable to large, productive biospheres than others. In particular, we hypothesize that planets with more efficient nutrient recycling via ocean upwelling will be better hosts for photosynthetic life than planets where nutrients will be sequestered at depth. Our results suggest that slowly rotating planets with higher surface pressure may support the most active biospheres because ocean upwelling—and thus nutrient recycling—is maximized under these conditions. Upwelling is also enhanced on planets somewhat larger than Earth, in salty oceans, and at intermediate positions within the Habitable Zone.

Higher orbital obliquity also promotes nutrient return from depth via greater upwelling. Even more intriguingly, large seasonal differences in the mixed layer on high obliquity planets may allow entrainment of previously exported nutrients into the mixed layer. This seasonality may also provide an efficient mechanism for the transfer of biosignatures produced in the deep ocean to the atmosphere, particularly given that high obliquity disfavors sea ice. High obliquity planets may thus host

particularly active life that may be uniquely detectable (Olson et al. 2018b), but strong seasonality in light availability may have additional biological consequences that are not considered here.

Although we did not explicitly vary land area or continental distribution, our results reveal that continents are also important. Coastal upwelling was the largest contributor to global upwelling in all of our model scenarios (Figures 4–9a). Moreover, in addition to promoting coastal upwelling and the recycling of nutrients from depth, continental weathering plays a key role in nutrient delivery to the ocean to balance nutrient burial in marine sediments on geologic timescales. This is in addition to the key role that continental weathering plays in climate regulation (Abbot et al. 2012). Although ocean worlds may meet existing definitions of habitability in some circumstances (Kite & Ford 2018), such planets will not be favorable targets for life detection owing to inevitable limitations on biospheric productivity in the absence of continents and associated nutrient fluxes via upwelling and weathering. Future work should explore the sensitivity of upwelling to alternate continental configurations and whether there exists optimal or problematic land distributions.

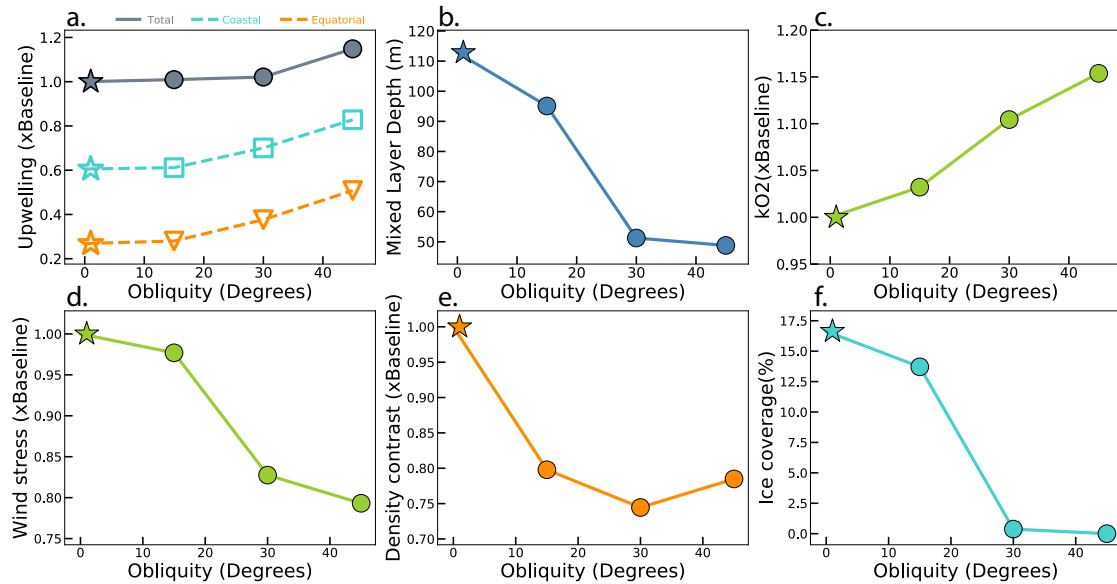


Figure 7. Ocean-atmosphere sensitivity to orbital obliquity, including: globally summed upwelling at the base of the mixed layer (a), global-average mixed layer depth (b), global-average oxygen gas exchange constant (c), global-average wind stress over ocean cells (d), global-average surface-to-deep density contrast (e), and global sea ice coverage (f). In each panel, the star denotes the baseline planet, which is generally Earth-like except that it has zero obliquity. Upwelling, k_{O_2} , wind stress, and the density contrast are normalized to their baseline values for ease of comparison. In (a), the filled grey circles represent the global total, the open blue squares are the coastal upwelling contribution to that total, and the open orange triangles are the equatorial upwelling component. All data are averaged over the last decade of the simulations.

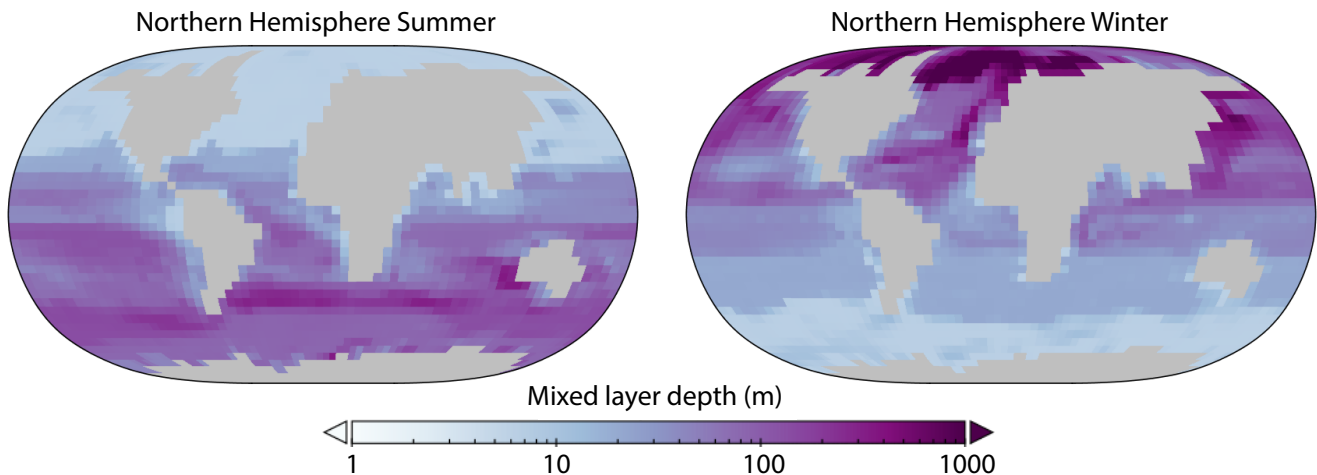


Figure 8. Seasonality in the mixed layer depth on a planet with 45° obliquity. The mixed layer depth locally varies by >2 orders of magnitude across the year. This seasonal deepening of the mixed layer allows entrainment of nutrients from depth.

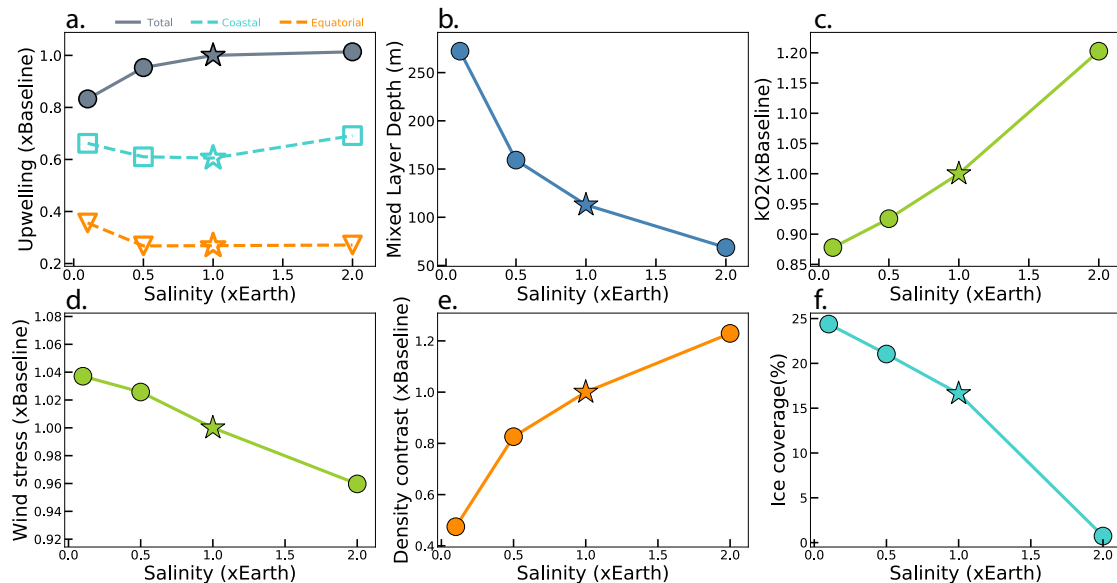


Figure 9. Ocean-atmosphere sensitivity to ocean salinity, including: globally summed upwelling at the base of the mixed layer (a), global-average mixed layer depth (b), global-average oxygen gas exchange constant (c), global-average wind stress over ocean cells (d), global-average surface-to-deep density contrast (e), and global sea ice coverage (f). In each panel, the star denotes the Earth-like baseline planet. Upwelling, k_{O_2} , wind stress, and the density contrast are normalized to their baseline values for ease of comparison. In (a), the filled grey circles represent the global total, the open blue squares are the coastal upwelling contribution to that total, and the open orange triangles are the equatorial upwelling component. All data are averaged over the last decade the simulations.

Intriguingly, the planetary parameters associated with greater upwelling also favor shallower mixed layer depths (with the exception of surface pressure), potentially leading to unexpected feedbacks between oceanographic phenomena and biogeochemical cycles. This interplay between the mixed layer depth and global upwelling deserves further attention, including explicit representation of the biological pump in a 3D biogeochemical model.

One important caveat for extending our results to constraints on exoplanet life detection is that the conditions that favor the maintenance of globally productive biospheres, such as nutrient recycling, may differ from the conditions that favor the origin of life. A planet must meet both criteria to host remotely detectable life. Our study focuses on the former and does not inform the latter.

4.2. Observational opportunities and challenges

Some of the planetary parameters that favor ocean upwelling and productive marine biospheres will be remotely observable. For example, Rayleigh scattering, pressure broadening of absorption bands, and pressure-sensitive dimers may reveal the presence of a dense atmosphere (Misra et al. 2014). In particular, although

N_2 itself is not spectrally active, the N_2 - N_2 collisional pair is spectrally recognizable and may be used to constrain N_2 levels (Schwieterman et al. 2015). Although high surface pressure is not a guarantee of a hospitable marine environment, the absence of a Rayleigh slope or N_2 - N_2 absorption should be considered a red flag that a target planet may have low surface pressure that may limit wind-driven upwelling, nutrient recycling in the ocean, and biospheric productivity. These planets may be more vulnerable to false negatives for life detection than planets with high surface pressure. Preliminary constraints on surface pressure thus offer a practical filter for prioritizing potentially habitable candidate planets for detailed characterization.

Time-resolved observations allow an opportunity to simultaneously probe rotation rate and to assess continentality by enabling longitudinal mapping of ocean vs. land (Cowan et al. 2009; Lustig-Yaeger et al. 2018), although surface mapping in this fashion will become increasingly challenging with decreasing rotation rates. Recognition of a short day-length or limited continentality may be indications of limited upwelling and an increased likelihood of a false negative that may motivate deprioritization in favor of planets with slower rotation rates and/or confirmed continentality.

Unfortunately, not all planetary parameters relevant for exo-oceanographic analysis will be readily observable. For example, exo-ocean salinity will likely be impossible to constrain observationally. The salinity of Earth’s ocean has changed dramatically in our history (e.g., Yang et al. 2017) and the salinities of other oceans in our own solar system apparently vary widely (e.g., Hand & Chyba 2007; Postberg et al. 2011; Mitri et al. 2014). Critically, we lack predictive models for these differences. Uncertainties regarding exo-ocean salinity must be considered in future attempts to simulate the climates of potentially habitable exoplanets (Cullum et al. 2016; Cael & Ferrari 2017; Del Genio et al. 2019).

4.3. Opportunities for future work

Our study did not exhaustively consider planetary parameter space and several opportunities for future work remain. In particular, we did not consider the impact of synchronous rotation and/or changes to the stellar spectrum, which may introduce the possibility of light (rather than nutrient) limited life (Lehmer et al. 2018). It is thus unclear how our results might be extended to M star systems. Extended periods of darkness are also a potential complicating factor on slowly rotating or high obliquity planets. We also did not explore the consequences of changing ocean depth, but note that dramatically differing ocean volumes are likely as a result of stochastic water delivery (Raymond et al. 2004) and may affect the interplay between the biological pump and ocean circulation. Finally, we have simply varied planetary parameters in isolation and it is possible that interactions between these parameters may amplify or mute differences in oceanographic properties. For example, we examined atmospheric mass and planetary mass independently but if they are positively correlated (Kopparapu et al. 2014) upwelling may be further enhanced on planets with larger radii.

Empirically, we know that planets with faster rotation rates, lower surface pressures, differing salinities, and lower stellar irradiation can be habitable given that all of these planetary parameters have evolved throughout Earth’s inhabitation history (reviewed by Olson et al. 2018a). The implications of our results for Earth system evolution may thus provide an exciting opportunity for future work. For example, several lines of evidence point to an origin of oxygenic photosynthesis very early in Earth’s history, potentially up to half a billion years before low-level oxygenation of the atmosphere during the Great Oxidation Event (Planavsky et al. 2014a), but the reason photosynthesis failed to oxygenate Earth’s atmosphere for so long is not understood. The reasons why post-GOE oxygen stabilized at levels much lower

than today are even more enigmatic (Planavsky et al. 2014b), but emerging models apparently require that primary productivity was lower than today for much of Earth’s history (e.g., Ozaki et al. 2019). Limited nutrients are thus widely invoked to explain limited surface oxygenation despite oxygen production (Reinhard et al. 2017b; Laakso & Schrag 2018; Ozaki et al. 2019), but these scenarios often lack physical mechanisms for limiting nutrient supply. Our results may provide a path forward: ocean upwelling and associated nutrient recycling processes may have simply been less efficient on an early Earth that rotated faster (Williams 2000), had lower surface pressure (Som et al. 2016), and orbited a fainter star compared to present day Earth (Gough 1981).

5. CONCLUSIONS

Ocean circulation controls the distribution and activity of life on Earth, and it modulates the communication between life in the ocean and the overlying atmosphere. We used an ocean-atmosphere GCM to explore oceanography, and the resulting ocean habitats, on planets differing from Earth. Our analysis focused on three ocean characteristics of biogeochemical significance, including: gas exchange kinetics, mixed layer depth, and upwelling at the base of the mixed layer. An intriguing result of our modeling is that the most Earth-like scenario was sub-optimal in many of our sensitivity experiments, introducing the possibility that true Earth twins may not be the most favorable targets for exoplanet life detection missions. Ocean circulation patterns on planets that rotate more slowly, have higher surface pressure, higher orbital obliquity, and saltier oceans than Earth may be more conducive to nutrient regeneration, biospheric productivity, and atmospheric biosignature accumulation than our own planet. Planets with larger radii may also be appealing candidates. Moving forward, we must make a distinction between worlds that meet some minimum criteria to be considered habitable (e.g., possessing liquid water) and those that will be hospitable to globally productive, *remotely detectable* life. Oceanographic phenomena should be at the center of such efforts.

ACKNOWLEDGEMENTS

S.L.O acknowledges support from the T.C. Chamberlin Postdoctoral Fellowship in the Department of the Geophysical Sciences at the University of Chicago. We thank the University of Chicago Research Computing Center for providing computing resources that were essential to this work.

REFERENCES

- Abbot, D. S., Cowan, N. B., & Ciesla, F. J. 2012, *The Astrophysical Journal*, 756, 178
- Ashkenazy, Y., Gildor, H., Losch, M., et al. 2013, *Nature*, 495, 90
- Cael, B. B., & Ferrari, R. 2017, *Geophysical Research Letters*, 44, 1886
- Cowan, N. B., Agol, E., Meadows, V. S., et al. 2009, *The Astrophysical Journal*, 700, 915
- Cullum, J., Stevens, D., & Joshi, M. 2014, *Astrobiology*, 14, 645
- Cullum, J., Stevens, D. P., & Joshi, M. M. 2016, *Proceedings of the National Academy of Sciences*, 113, 4278
- Del Genio, A. D., Way, M. J., Amundsen, D. S., et al. 2019, *Astrobiology*, 19
- Gough, D. O. 1981, *Sol. Phys.*, 74, 21
- Hand, K., & Chyba, C. 2007, *Icarus*, 189, 424
- Hu, Y., & Yang, J. 2014, *Proceedings of the National Academy of Sciences*, 111, 629
- Jansen, M. F. 2016, *Journal of Physical Oceanography*, 46, 1917
- Kang, W. 2019, *The Astrophysical Journal*, 876, L1
- Kaspi, Y., & Showman, A. P. 2015, *The Astrophysical Journal*, 804, 60
- Kasting, J. F., Whitmire, D. P., & Reynolds, R. T. 1993, *Icarus*, 101, 108
- Keles, E., Grenfell, J. L., Godolt, M., Stracke, B., & Rauer, H. 2018, *Astrobiology*, 18, 116
- Kite, E. S., & Ford, E. B. 2018, *The Astrophysical Journal*, 864, 75
- Komacek, T. D., & Abbot, D. S. 2019, *The Astrophysical Journal*, 871, 245
- Kopparapu, R. K., Ramirez, R. M., SchottelKotte, J., et al. 2014, *The Astrophysical Journal*, 787, L29
- Krissansen-Totton, J., Olson, S., & Catling, D. C. 2018, *Science Advances*, 4, eaao5747
- Laakso, T. A., & Schrag, D. P. 2018, *Global Biogeochemical Cycles*, 32, 486
- Large, W. G., McWilliams, J. C., & Doney, S. C. 1994, *Reviews of Geophysics*, 32, 363
- Lehmer, O. R., Catling, D. C., Parenteau, M. N., & Hoehler, T. M. 2018, *The Astrophysical Journal*, 859, 171
- Li, Z., & Cassar, N. 2017, *Biogeosciences*, 14, 5015
- Lustig-Yaeger, J., Meadows, V. S., Mendoza, G. T., et al. 2018, *The Astronomical Journal*, 156, 301
- Misra, A., Meadows, V., Claire, M., & Crisp, D. 2014, *Astrobiology*, 14, 67
- Mitri, G., Meriggiola, R., Hayes, A., et al. 2014, *Icarus*, 236, 169
- Olson, S. L., Kump, L. R., & Kasting, J. F. 2013, Special Issue dedicated to H.D. Holland: Evolution of the atmosphere and ocean through time, 362, 35
- Olson, S. L., Reinhard, C. T., & Lyons, T. W. 2016, *Proceedings of the National Academy of Sciences*, 113, 11447
- Olson, S. L., Schwieterman, E. W., Reinhard, C. T., & Lyons, T. W. 2018a, in *Handbook of Exoplanets*, ed. H. J. Deeg & J. A. Belmonte (Cham: Springer International Publishing), 1–37
- Olson, S. L., Schwieterman, E. W., Reinhard, C. T., et al. 2018b, *The Astrophysical Journal*, 858, L14
- Ozaki, K., Reinhard, C. T., & Tajika, E. 2019, *Geobiology*, 17, 3
- Planavsky, N. J., Asael, D., Hofmann, A., et al. 2014a, *Nature Geoscience*, 7, 283
- Planavsky, N. J., Reinhard, C. T., Wang, X., et al. 2014b, *Science*, 346, 635
- Postberg, F., Schmidt, J., Hillier, J., Kempf, S., & Srama, R. 2011, *Nature*, 474, 620
- Raymond, S. N., Quinn, T., & Lunine, J. I. 2004, *Icarus*, 168, 1
- Reinhard, C. T., Olson, S. L., Schwieterman, E. W., & Lyons, T. W. 2017a, *Astrobiology*, 17, 287
- Reinhard, C. T., Planavsky, N. J., Gill, B. C., et al. 2017b, *Nature*, 541, 386
- Robinson, T. D., Meadows, V. S., & Crisp, D. 2010, *The Astrophysical Journal*, 721, L67
- Rogers, L. A. 2015, *The Astrophysical Journal*, 801, 41
- Schmidt, G. A., Kelley, M., Nazarenko, L., et al. 2014, *Journal of Advances in Modeling Earth Systems*, 6, 141
- Schwieterman, E. W., Robinson, T. D., Meadows, V. S., Misra, A., & Domagal-Goldman, S. 2015, *The Astrophysical Journal*, 810, 57
- Schwieterman, E. W., Kiang, N. Y., Parenteau, M. N., et al. 2018, *Astrobiology*, 18, 663
- Som, S. M., Buick, R., Hagadorn, J. W., et al. 2016, *Nature Geoscience*, 9, 448
- Sverdrup, H. U. 1953, *ICES Journal of Marine Science*, 18, 287
- Wanninkhof, R. 2014, *Limnology and Oceanography: Methods*, 12, 351
- Way, M. J., Del Genio, A. D., Aleinov, I., et al. 2018, arXiv:1808.06480 [astro-ph], arXiv: 1808.06480
- Way, M. J., Aleinov, I., Amundsen, D. S., et al. 2017, *The Astrophysical Journal Supplement Series*, 231, 12
- Williams, G. 2000, *Reviews of Geophysics*, 38, 37
- Yang, J., Abbot, D. S., Koll, D. D. B., Hu, Y., & Showman, A. P. 2019, *The Astrophysical Journal*, 871, 29

Yang, J., Jansen, M. F., Macdonald, F. A., & Abbot, D. S.
2017, *Geology*, 45, 615

Zhang, J., & Rothrock, D. 2000, *Journal of Geophysical
Research: Oceans*, 105, 3325